

Bilevel Generative Learning for Low-Light Vision

Yingchi Liu

Dalian University of Technology
yingchi@mail.dlut.edu.cn

Zhu Liu

Dalian University of Technology
liuzhu@mail.dlut.edu.cn

Long Ma

Dalian University of Technology
malone94319@gmail.com

Jinyuan Liu

Dalian University of Technology
atlantis918@hotmail.com

Xin Fan

Dalian University of Technology
xin.fan@dlut.edu.cn

Zhongxuan Luo

Dalian University of Technology
zxluo@dlut.edu.cn

Risheng Liu*

Dalian University of Technology
Peng Cheng Laboratory
rslu@dlut.edu.cn

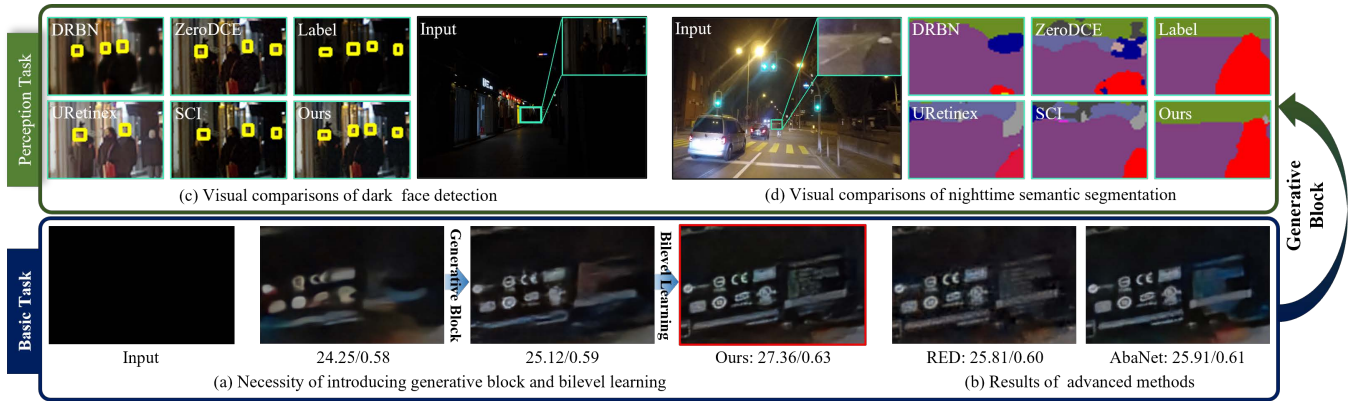


Figure 1: Illustration of the core unified framework for low-light vision tasks. We first demonstrate the necessity of introducing generative block from the RAW domain and further drastically improve the performance based on bilevel learning in (a) based on the basic image enhancement task. Then we compare with the advanced enhanced methods in (b). By plugging the pretrained generative block, significant promotion can be observed from the low-light face detection and nighttime semantic segmentation tasks in (c) and (d).

ABSTRACT

Recently, there has been a growing interest in constructing deep learning schemes for Low-Light Vision (LLV). Existing techniques primarily focus on designing task-specific and data-dependent vision models on the standard RGB domain, which inherently contain latent data associations. In this study, we propose a generic low-light vision solution by introducing a generative block to convert data from the RAW to the RGB domain. This novel approach connects diverse vision problems by explicitly depicting data generation, which is the first in the field. To precisely characterize the

*Corresponding author: Risheng Liu

Permission to make digital or hard copies of all or part of this work for personal or classroom use is granted without fee provided that copies are not made or distributed for profit or commercial advantage and that copies bear this notice and the full citation on the first page. Copyrights for components of this work owned by others than ACM must be honored. Abstracting with credit is permitted. To copy otherwise, or republish, to post on servers or to redistribute to lists, requires prior specific permission and/or a fee. Request permissions from permissions@acm.org.
MM '23, October 29–November 3, 2023, Ottawa, ON, Canada.

© 2023 Association for Computing Machinery.
ACM ISBN 979-8-4007-0108-5/23/10...\$15.00
<https://doi.org/10.1145/3581783.3611859>

latent correspondence between the generative procedure and the vision task, we establish a bilevel model with the parameters of the generative block defined as the upper level and the parameters of the vision task defined as the lower level. We further develop two types of learning strategies targeting different goals, namely low cost and high accuracy, to acquire a new bilevel generative learning paradigm. The generative blocks embrace a strong generalization ability in other low-light vision tasks through the bilevel optimization on enhancement tasks. Extensive experimental evaluations on three representative low-light vision tasks, namely enhancement, detection, and segmentation, fully demonstrate the superiority of our proposed approach. The code will be available at <https://github.com/Yingchi1998/BGL>.

CCS CONCEPTS

• **Computing methodologies** → **Computer vision.**

KEYWORDS

Low-light vision, RAW generative block, bilevel generative learning

ACM Reference Format:

Yingchi Liu, Zhu Liu, Long Ma, Jinyuan Liu, Xin Fan, Zhongxuan Luo, and Risheng Liu. 2023. Bilevel Generative Learning for Low-Light Vision. In *Proceedings of the 31st ACM International Conference on Multimedia (MM '23)*, October 29–November 3, 2023, Ottawa, ON, Canada. ACM, New York, NY, USA, 9 pages. <https://doi.org/10.1145/3581783.3611859>

1 INTRODUCTION

Due to various forms of degradation, such as low illumination, color distortion, low contrast, and imaging noises, low-light vision tasks have become more challenging and have received widespread attention [9, 10, 13, 25, 26, 48]. The inadequate representation of scenes with low-light observation reduces the perception of the human visual system [10, 16, 21, 28] and severely hinders the feature utilization and performance of various scene perception tasks. Therefore, improving visual quality and investigating effective features for downstream scene understanding are significant in real-world applications, e.g., autonomous sensing [11] and robotic operations [32].

In recent years, significant advances have been made in learning-based schemes for low-light vision tasks. These approaches aim to highlight sufficient scene information under severe illumination conditions. For visual enhancement, Retinex-based decomposition principles that estimate illumination and recover normal-light reflection are widely utilized [26, 27, 53]. For scene perception [19, 20, 23, 24], approaches such as bi-directional high-low level adaptation [40] and recurrent exposure generation [18] have been proposed. These schemes achieve excellent through task-specialized schematic design and data-driven optimization under RGB domain.

However, the heuristic and independent design of current low-light vision tasks complicates unified modeling, making it challenging to realize diverse purposes of low-light vision under a versatile framework. Low-light images based on RGB formation inevitably suffer from strong noise and color distortion, which limits their performance at its core.

Owing to the higher bit depth to capture features, many learning-based methods aim to investigate the low-light scene information from RAW domain for perception tasks [29, 30, 38, 45]. Despite the presence of large noise from hardware device, the original RAW formation also provides the sufficient scene information. These methods design the specialized solutions for specific task goals, which cannot flexible generalize into other low-light vision tasks without modular-style design. Different from existing methods, we endow the adaptive data generation from RAW to establish the connection of diverse vision tasks, which is key to improving the performances for diverse perception tasks.

To partially mitigate the above issues, we propose Bilevel Generative Learning (BGL) to uniformly solve various low-light vision tasks under the RAW domain. Within this formulation, we introduce the RAW-based generation as the goal and the low-light vision is cast as a constraint. This bilevel generative learning can naturally provide a new perspective to describe the implicit relationship between the image generated from RAW data and performance of low-light vision. In addition, we construct two optimization strategies to provide efficient solutions including truncated and implicit bilevel generative learning for real-world practices. These training strategies are both with high efficiency compared with mainstream bilevel solutions and avoid any needs to fine-tune with downstream

low-light vision networks. Note that the generative block trained by bilevel learning is versatile enough to promote the performances of other low-light vision tasks. As shown in Fig. 1, our scheme can realize the significant improvement for diverse tasks (i.e., image enhancement, detection and segmentation). The main contributions of this work can be summarized as:

- To the best of our knowledge, we are the first to provide a versatile framework to address low-light vision perception tasks under the support of generative procedure from RAW space. It not only endows task guidance for generating data, but also boosts the performance of vision tasks.
- In order to exploit the latent connection between data generation and task-specific parameters, we provide a bilevel generative learning paradigm to effectively model their inner correspondence and acquire the data generation with strong generalized capabilities for diverse vision tasks.
- To satisfy different demands in real-world practice, we develop two strategies for BGL, including a truncated BGL for alleviating computation costs and an implicit BGL for high accuracy, which provide effective and precise responses for the data generation learning.
- Comprehensive experiments have elaborated the remarkable improvements for various low-light visual perception tasks, achieving promising results against advanced methods. We also make extensive analysis in terms of our proposed method to verify our effectiveness.

2 RELATED WORKS

In this part, we first briefly review the current development of low-light vision based on RGB and RAW domains.

RGB-based LLV. Recently, existing low-light enhancement methods designed heuristic network structure based on data-driven for specific low-light scenes and yielded better results for image restoration. Among them, Retinex-theory has been the mainstream methodology for low-light enhancement. For instance, image decomposition scheme is proposed to simultaneously optimize the illumination and reflections. The work [53] introduces the decomposition mechanisms to estimate the illumination and reflectance at feature domain. As for scene perception, target-specific (e.g., face) low-light object detection is a typical task. [40] designed a dual-direction adaptation framework with a interactive bidirectional high-low level adaptation, which can extract effective information for high level from the low level module. In summary, learning-based schemes constructed independent architectures and training strategies to achieve promising results with high efficiency. One major challenge is the difficulty to formulate these low-light vision tasks with a principled unified framework, due to the independent design of these schemes. In our scheme, we aims to seek data connection of these tasks to design a versatile framework with a suitable training strategy.

RAW-based LLV. Since RAW images contain comprehensive information with untreated scene representation. Several works have pioneered to simulate the RAW-to-RGB mapping to address diverse vision tasks. Specifically, as for low-light vision enhancement, SID-firstly proposed a landmark cornerstone with sufficient RAW-RGB

pairs under low-light scenes with different exposure time. Moreover, DID replaces the U-Net structure with the cascaded residual blocks, in order to preserve the texture details with the same resolution. Lastly, there are also some schemes to construct low-weight architectures, such as LLPackNet, RED and SGN, leveraging the low-resolution operating, multi-scale processing and self-guided mechanisms respectively. Based on the unprocessing technique, Chen *et.al* propose the low-light RAW-input instance segmentation algorithm [2] based on a low-light RAW synthetic pipeline from RGB domain. Inspired by this work, we can further introduce the unprocessing to mitigate the shortage of RAW datasets under low-light environment. These learnable transformation schemes rely on data-driven, which achieve high superiority of performance.

3 PROPOSED METHOD

In this part, we first present the core motivation, introducing the data generation block from the RAW data to integrate the solution of diverse low-light vision tasks. Then we formulate the data generative block and downstream vision tasks based on the bilevel generative modeling.

3.1 Low-light Vision with Generative Block

The mainstream methodology to address low-light vision tasks is to design independent architectures for specific training data. In this way, due to the distinct principles to design architectures, it is difficult to introduce a unified scheme to take diverse low-light vision tasks under comprehensive consideration. From the intuitive viewpoint, we can observe that these learning-based methods actually share the similar data dependence, i.e., the low-light observations. Thus, how to investigate connections among low-light tasks from data generation perspective is a potential direction.

In this manuscript, we introduce a generative block from RAW space for vision task. It is noticeable that, in essence, generative block is task-agnostic, which only targets to establish the mapping between RAW and RGB images. In a word, data generation does not have the strong correlation with specific vision tasks. In this way, for diverse low-light vision tasks, we can introduce the learnable data generation to construct a common dependence and further formulate the unified framework to bridge these vision tasks. Furthermore, the original information from RAW domain is not corrupted. We can extract efficient features from RAW data to further improve the performance of vision tasks.

In detail, we denote \mathbf{z} , \mathbf{x} and \mathbf{y} are inputs from RAW, RGB space and task-specific outputs, respectively. The complete framework can be formulated as $\mathcal{N} := \mathcal{F} \circ \mathcal{G}$, where \mathcal{F} and \mathcal{G} are the network of data generation and low-light vision tasks. The whole formation can be written as:

$$\begin{cases} \mathbf{x} = \mathcal{F}(\mathbf{z}; \omega), \\ \mathbf{y} = \mathcal{G}(\mathbf{x}; \theta), \end{cases} \quad (1)$$

where ω and θ are the corresponding parameters. These details about the network implementation are reported at Section.3.5.

In this part, we construct a cascade framework to formulate their forward data flow. The direct heuristic optimization strategy is to perform the end-to-end learning. However, we argue that the straightforward optimization cannot model the complicated

relationship between data generation and vision tasks. The straightforward training only consider their goal independently, without the formulation of their coupled influences. Thus, how to depict their latent correspondence becomes another challenging issue.

3.2 Modeling with Bilevel Optimization

In this part, we demonstrate how the bilevel modeling relates to the formulation between generative learning and parameter learning of low-light vision. Bilevel modeling is a technique to involve hierarchical optimization tasks, where the lower-level task is nested in the upper-level optimization. Analogy with effective practices on generative adversarial networks [6, 22] and adversarial attacks [52], we can naturally discover the core relationship between data generation and task-specific parameter learning.

Intuitively, the data generation from RAW domain can be considered as one ‘‘Generator’’, to provide inputs satisfied for downstream low-light vision tasks. On the other hand, the role of network for low-light vision can be viewed as the ‘‘Discriminator’’, to provide the task guidance and feedback in order to adjust the learning procedure of generative block. Importantly, it supplies a more powerful understanding compared with naive end-to-end learning and new perspective to model the correspondence between training data and network parameters.

To make the above intuition clear, the bilevel modeling between data generation and parameter learning can be formulated as:

$$\min_{\omega} \mathcal{L}_{\mathcal{F}}(\mathcal{F}(\mathbf{z}; \omega) \circ \mathcal{G}(\mathbf{x}; \theta^*)), \quad (2)$$

$$\text{s.t. } \theta^* = \arg \min_{\theta} \mathcal{L}_{\mathcal{G}}(\mathcal{G}(\mathbf{x}; \theta(\omega))), \quad (3)$$

where $\mathbf{x} = \mathcal{F}(\mathbf{z}; \omega^*)$. We define the parameters of generative block ω as the related hyper-parameters to learn the scene-agnostic feature representation. $\mathcal{L}_{\mathcal{F}}$ denotes the task-specific loss on the validation dataset to optimize the generative block. $\mathcal{L}_{\mathcal{G}}$ represents the optimization objective for the visual task module. We introduce the vision task as constraints to utilize more task-related responses. Furthermore, this formulation is flexible enough to replace effective learnable modules for \mathcal{F} and \mathcal{G} with strong versatility. Different from other works that focus on network design, we put more attention on characterizing the correspondence between informative data generation and low-light vision tasks.

3.3 Bilevel Generative Learning

In literature, amounts of computation strategies are proposed to address these constrained modeling. However, due to the complicated nested formulation of Eq. (2) and Eq. (3), parameters of generative block ω is actually embedded into the optimization of vision tasks. The solving procedure of current bilevel optimization always needs massive computation resource, limiting their applications on the simple tasks. Specifically, the bottleneck of optimization is to introduce the task-related response based on \mathcal{G} , when computing the gradient of \mathcal{F} , which can be formulated as

$$\mathbf{G}_{\mathcal{F}} := \nabla_{\omega} \mathcal{L}_{\mathcal{F}} + \underbrace{\nabla_{\theta} \mathcal{L}_{\mathcal{F}} \nabla_{\omega} \theta(\omega)}_{\text{Second-order gradient}}. \quad (4)$$

The first term represents the direct gradient for generative block. The second term reveals the task-specific responses of \mathcal{F} for downstream vision tasks. Thus, this provides us with a more intuitive view to understand the complicated connection between ω and θ .

Existing methods cannot satisfy the demand of low cost or high accuracy to solve our model. In this part, we propose two effective strategies to approximate the second term of Eq. (4), which provide efficient solutions for different demands (*i.e.*, low computation cost and high performance). The practical solutions for different demands are summarized at Alg. 1 and Alg. 2.

Algorithm 1 Truncated Bilevel Generative Learning (TBGL).

Require: Inputs from RAW domain \mathbf{z} , loss function $\mathcal{L}_{\mathcal{F}}$ and $\mathcal{L}_{\mathcal{G}}$ and other necessary hyper-parameters.

- 1: RGB output \mathbf{x} and \mathbf{y} .
- 2: Pretrain the $\mathcal{F}(\mathbf{z}; \omega) \circ \mathcal{G}(\mathbf{x}; \theta)$ for initializing θ and ω .
- 3: Joint optimizing \mathcal{F} and \mathcal{G} utilizing $\mathcal{L}_{\mathcal{G}}$.
- 4: % Solving the bilevel modeling.
- 5: **while** not converged **do**
- 6: % Updating the network of vision task \mathcal{G} (with one step).
- 7: $\theta \leftarrow \theta - \nabla_{\theta} \mathcal{L}_{\mathcal{G}}(\mathcal{G}(\mathbf{x}; \theta(\omega)))$.
- 8: % Updating the network of generative learning \mathcal{F} .
- 9: Calculating gradient $\mathbf{G}_{\mathcal{F}}$ with TBGL (Eq. (5)).
- 10: $\omega \leftarrow \omega - \mathbf{G}_{\mathcal{F}}$.
- 11: **end while**
- 12: **return** ω^* and θ^* .

3.3.1 Truncated BGL for Lower Cost. We first introduce a truncated BGL to reduce the computation cost. In detail, this strategy is based on the one-step forward model [26], which is truncated with recurrent updates of \mathcal{G} ($\mathbf{k} = 1$ in the Alg. 1). Denoted that $\theta' = \theta - \eta \nabla_{\theta} \mathcal{L}_{\mathcal{G}}$, the gradient of \mathcal{F} can be written as $\nabla_{\omega} \mathcal{L}_{\mathcal{F}} - \eta \nabla_{\omega}^2 \mathcal{L}_{\mathcal{G}} \nabla_{\theta'} \mathcal{L}_{\mathcal{F}}$. First-order based approximation is widely used, which can significantly circumvent the huge memory utilization for expensive hessian matrix and improve computation efficiency by approximating the second-order gradient. By utilizing the finite difference approximation, the second term can be computed as:

$$\nabla_{\omega, \theta}^2 \mathcal{L}_{\mathcal{G}} \nabla_{\theta'} \mathcal{L}_{\mathcal{F}} \approx \frac{\nabla_{\omega} \mathcal{L}_{\mathcal{G}}(\omega; \theta^+) - \nabla_{\omega} \mathcal{L}_{\mathcal{G}}(\omega; \theta^-)}{2\delta}, \quad (5)$$

where δ is a constant and $\theta^{\pm} = \theta \pm \delta \nabla_{\theta} \mathcal{L}_{\mathcal{G}}$. In this way, the solution of Eq. (4) actually contains three first-order gradient computation for ω . Thus the simplification only perform one-step update, which drastically reduce the computation cost. However, though highly efficiency obtained, this strategy is restricted to the one-step back-propagation for sufficiently learning the conversion \mathcal{F} . In other words, Truncated BGL (TBGL) cannot guarantee the performance stably, without reasonable responses from well-trained low-light vision tasks. Thus, we introduce another strategy to provide higher performance to solve the Eq. (4). In the next part, we will explore the concrete computation learning strategy to address this bilevel optimization objective.

3.3.2 Implicit BGL for Higher Accuracy. Introducing the Gaussian-Newton method to approximate the second-order matrix for addressing Generative Adversarial Networks (GANs) and continuous

learning is introduced in [22]. This strategy is based on the implicit gradient approximation, where the implicit function theory is employed to fastly estimate the coupled second-order term (denoted as $\mathcal{G}_{\mathcal{C}}$). Based on the implicit function assumption, $\nabla_{\theta} \mathcal{L}_{\mathcal{G}} = 0$, we can have $\nabla_{\omega} \theta(\omega) = -\nabla_{\theta, \theta}^2 \mathcal{L}_{\mathcal{G}}^{-1} \nabla_{\omega, \theta}^2 \mathcal{L}_{\mathcal{G}}$. Assuming that $\nabla_{\omega, \theta}^2 \mathcal{L}_{\mathcal{G}}$ is transposeable, the coupling gradient $\mathcal{G}_{\mathcal{C}}$ can be written as follows:

$$\mathcal{G}_{\mathcal{C}} = -\nabla_{\omega, \theta}^2 \mathcal{L}_{\mathcal{G}}(\omega, \theta)^{\top} \nabla_{\theta, \theta}^2 \mathcal{L}_{\mathcal{G}}(\omega; \theta)^{-1} \nabla_{\theta} \mathcal{L}_{\mathcal{F}}. \quad (6)$$

This formulation actually have two second-order derivatives (Hessian and its inverse). Utilizing the inspiration of Gauss-Newton method, which utilize the outer-product-based approximations. This term can be computed as:

$$\nabla_{\theta, \theta}^2 \mathcal{L}_{\mathcal{G}}(\omega; \theta) \approx \nabla_{\theta} \mathcal{L}_{\mathcal{G}}(\omega; \theta) \nabla_{\theta} \mathcal{L}_{\mathcal{G}}(\omega; \theta)^{\top}. \quad (7)$$

$$\nabla_{\omega, \theta}^2 \mathcal{L}_{\mathcal{G}}(\omega; \theta) \approx \nabla_{\theta} \mathcal{L}_{\mathcal{G}}(\omega; \theta) \nabla_{\omega} \mathcal{L}_{\mathcal{G}}(\omega; \theta)^{\top}. \quad (8)$$

This way of gradient approximation converts the two second-order Hessian matrix into a simple product operation of the first-order derivation, which can greatly improve the computation efficiency. The coupling gradient $\mathcal{G}_{\mathcal{C}}$ can be obtained as follows:

$$\mathcal{G}_{\mathcal{C}} \approx -\frac{\nabla_{\theta} \mathcal{L}_{\mathcal{F}}(\omega; \theta)^{\top} \nabla_{\theta} \mathcal{L}_{\mathcal{G}}(\omega; \theta)}{\nabla_{\theta} \mathcal{L}_{\mathcal{G}}(\omega; \theta)^{\top} \nabla_{\theta} \mathcal{L}_{\mathcal{G}}(\omega; \theta)} \nabla_{\omega} \mathcal{L}_{\mathcal{G}}(\omega; \theta). \quad (9)$$

Different from the above truncated BGL, which only updates one step of the lower-level objective, we set more training steps to update \mathcal{F} for the convergence and provide more accurate responses for the generative learning. In this way, we can avoid the limitation of one-step updating. Similarly, we only need to compute several first-order gradients rather than Hessian products. Network of LLV can be trained to approximate the optimal, which can offer more precise response. Thus, IBGL can guarantee the high performance of the solution. But this strategy cannot maintain the efficiency and needs the amounts of updating for \mathcal{G} compared with TBGL.

Algorithm 2 Implicit Bilevel Generative Learning (IBGL).

Require: Same as the Algorithm 1.

- 1: % Warm start phase.
- 2: Joint optimizing \mathcal{F} and \mathcal{G} utilizing $\mathcal{L}_{\mathcal{G}}$.
- 3: **while** not converged **do**
- 4: % Updating the network of vision task \mathcal{G} with \mathbf{k} steps.
- 5: **for** $i = 1$ to \mathbf{k} steps **do**
- 6: $\theta \leftarrow \theta - \nabla_{\theta} \mathcal{L}_{\mathcal{G}}(\mathcal{G}(\mathbf{x}; \theta(\omega)))$;
- 7: **end for**
- 8: % Updating the network of generative learning \mathcal{F} .
- 9: Calculating gradient $\mathbf{G}_{\mathcal{F}}$ with IBGL(Eq. (9)).
- 10: $\omega \leftarrow \omega - \mathbf{G}_{\mathcal{F}}$.
- 11: **end while**
- 12: **return** ω^* and θ^* .

3.4 Discussion

It is worth noting that this is the first work to model the RAW-based data generation with vision tasks from a generic bilevel optimization perspective. Instead of introducing a unique design or modules in the RAW processing, we are investigating the data generation

from RAW space as a hyper-parameter optimization and considering the constraints from low-light vision to assist the learning of data generation.

3.5 Architectures and Loss Functions

In detail, we introduce a U-Net type encoder-decoder to construct the neural architecture of generative block, which contains four layers of convolutions to extract the multi-scale features and introduce the skip connections to fuse features from encoder and decoder. We consider two classical low-light vision tasks, *i.e.*, visual enhancement and object detection. As for the visual enhancement, designating the enhancement module as \mathcal{G} , we introduce the Retinex theory [41] to estimate the normal illumination with a light-weight architecture design. We establish three cascaded convolution layers to generate the four three-channel illumination, which couples with one single skip connection. Visual enhancement module can be formulated as $y = x \odot \mathcal{G}(x, \theta)$. As for the dark face detection, we introduce a well-known face detector DSFD [17] as \mathcal{G} . Noting that, our framework also can realize other low-light scene perception tasks with strong generalization. The L1 loss is defined as $\mathcal{L}_{\mathcal{F}}$ in the generative block. We utilize the self-supervised illumination learning loss to define $\mathcal{L}_{\mathcal{G}}$ on enhancement. Multibox objective learning loss is utilized to define $\mathcal{L}_{\mathcal{G}}$ on detection.

4 EXPERIMENTS

4.1 Implementation Details

Benchmarks description and metrics. We utilized three datasets to conduct our experiments, including SID [1], DARK FACE [47] and ACDC [36]. For the SID dataset, we sampled 2697 short-exposure images and 231 long-exposure reference images based on the Sony $\alpha 7S$ II sensor for training, and 598 image pairs for testing. We randomly selected 400 pairs of data for training and 106 pairs for testing on the ACDC dataset. For the DARK FACE dataset, we used 5000 images for training and 1000 images for testing in the context of object detection. It is worth noting that due to the unavailability of raw data on the DARK FACE dataset, we obtained raw data by means of an unprocess [2] approach. For the image enhancement, we used eight metrics including PSNR, SSIM, LPIPS [50], VIF [37], FSIM [49], BRISQUE [34], NIQE [35] and LOE [39]. The metrics of mAP and mIOU are used for dark face detection and low-light semantic segmentation respectively.

Parameter settings. During the training phase for the enhancement task, we applied data augmentation methods throughout the training stages and cropped the images to a size of 512×512 for the SID dataset. We set the initial learning rate to 10^{-4} during the warm start phase. In the bilevel training phase, we used the IBGL solver to achieve better performance. The learning rate of the upper model \mathcal{F} was set to 3×10^{-3} and decayed to 5×10^{-6} , while the learning rate of the lower model \mathcal{G} was set to 3×10^{-3} and decayed to 3×10^{-5} . With a batch size of 2, we set $k = 80$ iterations for optimizing the generative block and updating the parameters of the underlying model at each iteration.

For the generative block trained on detection task, we use SGD optimizers with an initial learning rate of 3×10^{-3} and 5×10^{-4} for generative block and detection model with 5e-4 weight decay and 0.9 momentum for both optimizers. The input images were cropped

to a size of 640×640 and the batch size was set to 8. In the bilevel training phase, we set $k = 30$. While training the segmentation task, the batch size is changed to 5 and the initial learning rate of the optimizer is set to 0.1. In the process of training the generation block on the enhancement task, the ADAM optimizer with parameters (0.9, 0.999) and initial learning rate of 3×10^{-3} is used for enhancement model. The following parameter configurations remain unchanged from the previous section. All experiments were performed on an NVIDIA RTX 3090 GPU using PyTorch framework.

4.2 Low-Light Image Enhancement

Qualitative comparison. Meanwhile, we also make comparisons among these methods in Fig. 2. There are three discriminative advantages. Firstly, our approach efficiently preserves the texture details present in the image, as shown in the zoom-out region of the second row, the results generated by AbaNet and SGN exhibit obvious texture detail distortion and our findings demonstrate the ability to depict a greater level of detail. Secondly, Our method preserves the natural colour distribution, *e.g.*, in the case of glass and trademark. Although RED recovers the clear background with vivid colours, the texture details severely corrupted. Thirdly, our approach can effectively reduce a significant amount of noise from the image, as shown in the zoom-out region of the first row, in comparison to the outcomes produced by RED, our results exhibit a higher level of clarity. Additionally, the results of our method exhibit abundant textural details.

Quantitative comparison. We performed a comprehensive evaluation of various methods on the SID, including SID [1], SGN [7], DID [33], LLPack [14], RED [15], RawFormer [44] and AbaNet [5]. We observed that our approach achieves significant improvements over RED method, with a 0.31dB increase in PSNR and the lowest perceptual errors based on LPIPS. A higher PSNR value indicates that the restored image is more similar to the ground truth image on pixel intensity. LPIPS measures the perceptual similarity incline with human visual perception.

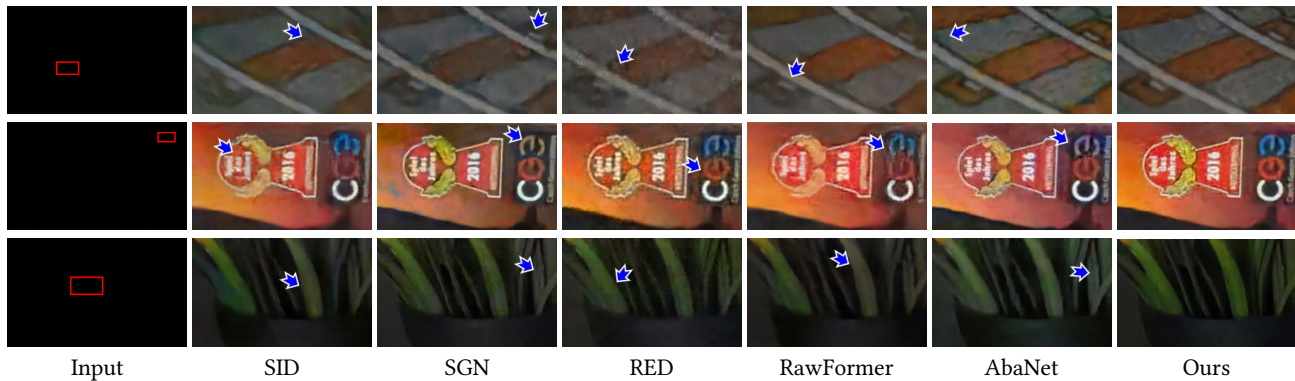
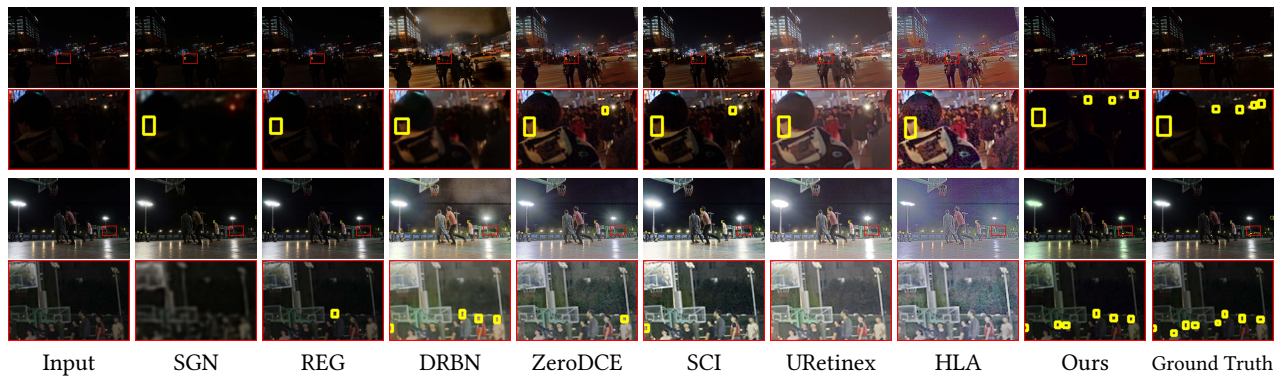
4.3 Dark Face Detection

Qualitative comparison. Fig. 3 showcases visual comparisons with advanced methods. For the enhanced images, although they exhibit noticeable enhancement effects, they may still fail to detect relatively small faces. In contrast, our method can effectively detect smaller faces and significantly improve precision, particularly in challenging scenes, for example, crowded in the distance. In the last row of images, overexposed images such as HLA can be observed, and these can lead to a reduction in detection accuracy. Furthermore, compared to the "SID +detection" method, our final results retain more texture detail information.

Quantitative comparison. We first plotted the Precision-Recall curve in Fig. 4 to demonstrate the superiority of our method. In comparison to various methods, including two "raw+detection" methods (SID, SGN), "enhancement+detection" methods (REG, FIDE [43], KinD [51], EnGAN [12], RetinexNet [41], DRBN [46], ZeroDCE [8], SCI [31] and URetinex [42]), all based on the same detector DSFD [17], as well as three face detection methods, MAET [4], REG [18] and HLA [40]. Our method improves mAP by 3.29% and

Table 1: Quantitative results of low-light enhancement on the SID dataset.

Method	SID <i>CVPR'2018</i>	SGN <i>ICCV'2019</i>	DID <i>ICME'2019</i>	LLpack <i>BMVC'2020</i>	RED <i>CVPR'2021</i>	RawFormer <i>SPL'2022</i>	AbaNet <i>CVPR'2022</i>	Ours –
PSNR \uparrow	28.262	26.883	28.814	27.944	28.811	28.483	29.011	29.122
SSIM \uparrow	0.763	0.753	0.767	0.753	0.744	0.765	0.768	0.769
LPIPS \downarrow	0.439	0.469	0.440	0.768	0.497	0.441	0.444	0.432
VIF \uparrow	0.917	0.927	0.909	0.388	0.890	0.951	0.960	0.923
FSIM \uparrow	0.930	0.923	0.930	0.680	0.921	0.844	0.937	0.931
BRISQUE \downarrow	28.726	29.429	29.427	35.544	27.653	27.706	27.702	27.603

**Figure 2: Visual comparison against state-of-the-art low-light image enhancement approaches on the SID dataset.****Figure 3: Visual comparison results against state-of-the-art low-light image enhancement approaches on the DARK FACE.**

7.98% compared to “SCI+detection” and “URetinex+detection”. In a word, our method achieves the best detection precision.

4.4 Nighttime Semantic Segmentation

Qualitative comparison. We also compared our method with other enhanced methods. DeepLabV3+ [3] serves as the baseline model for segmentation task, and the outcomes of all comparative methods are derived in the same manner with the dark face detection. As shown in Fig. 7, compared with other methods, our scheme can accurately segment the edges of different objects, such as roads, sidewalks, and street light signs. In the first row of images, our visuals appear more natural and accurate, thanks to the mitigation

of severe artifacts and color distortion issues that exist in other results, such as SCI and URetinex. It is obviously that our scheme can obtain more accurate segmentation results.

Quantitative comparison. Table. 2 demonstrates the quantitative results on the nighttime semantic segmentation task. Obviously, our results exhibits a 1.93% mIOU improvement over SCI method. Additionally, our segmentation results exhibit greater accuracy for specific categories, including building, wall, and fence. For example, our method achieves a 17.40% mIOU higher score than SUC in segmenting fence, and a 0.5 mIOU higher score than URetinex in segmenting building. In a word, our results are more superior from the statistical perspective.

Table 2: Qualitative results compared with state-of-the-art methods on ACDC dataset. The best result is in red whereas the second one is in blue. The symbol set {RO, SI, BU, WA, FE, PO, TL, TS, VE, TE, SK, PE, RI, CA, TR, BI} represents {road, sidewalk, building, wall, fence, pole, traffic light, traffic sign, vegetation, terrain, sky, person, rider, car, train, bicycle}.

Methods	RO	SI	BU	WA	FE	PO	TL	TS	VE	TE	SK	PE	RI	CA	TR	BI	mIOU \uparrow
RetineNet	89.43	61.00	74.21	32.86	28.13	42.43	49.82	25.71	65.87	8.63	77.37	21.55	13.88	54.88	67.44	8.20	41.96
DRBN	90.51	61.51	72.81	30.16	32.54	44.56	47.63	27.22	65.74	10.20	76.56	24.28	13.24	55.47	71.12	11.94	43.38
FIDE	90.00	60.74	72.81	32.48	34.13	43.32	47.91	26.10	67.04	13.79	78.00	26.57	5.80	57.10	71.04	12.48	43.47
KinD	90.00	61.02	73.25	31.96	32.89	43.58	47.91	27.76	65.55	13.33	77.47	22.83	8.10	55.16	74.57	11.56	43.00
EnGAN	89.74	58.96	73.56	32.84	31.82	44.74	42.75	26.28	67.33	14.28	77.88	25.00	10.69	59.00	71.28	7.80	43.85
SSINet	89.66	59.38	72.58	29.90	31.72	45.46	43.90	24.50	66.75	10.68	78.39	22.82	0.22	52.67	71.12	5.48	41.47
ZeroDCE	89.63	59.93	73.94	32.65	31.76	44.35	46.27	25.88	67.20	14.67	79.10	24.73	7.76	13.29	66.83	13.99	43.42
SCI	92.29	59.93	69.22	39.78	39.56	37.18	44.78	33.72	39.82	5.03	67.78	26.03	30.03	59.44	70.91	7.89	44.06
SUC	92.40	69.55	76.00	39.57	34.70	44.70	54.15	39.10	67.07	11.22	79.32	25.24	10.44	69.77	84.76	27.43	44.34
URetinex	90.38	65.59	75.81	40.10	35.95	43.59	53.51	40.79	65.07	8.30	78.81	26.95	13.48	67.31	80.90	25.58	43.82
Ours	93.06	70.27	76.31	41.76	40.74	44.08	53.61	34.40	68.53	9.40	79.38	27.19	8.01	66.90	85.05	45.76	44.91

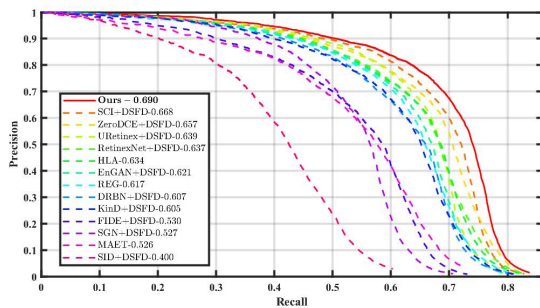


Figure 4: Precision-Recall curve of detection results on the DARK FACE dataset.



Figure 5: Visual enhancement qualitative results based on SID dataset among various training strategy.

4.5 Framework Evaluation

Evaluation of the generative block. We first analyzed the effectiveness of our proposed generative block approach (referred to as GB). For visual enhancement, as shown in first figure, the PSNR with GB improved significantly by 0.87 dB and restored more English alphabet compared with the framework without GB. Both the numerical and visual comparisons clearly demonstrate the crucial role of the GB in providing task-friendly observations, underscoring the effectiveness of our proposed GB.

Generalization of bilevel learning. We examine the inherent characteristics of both components of the generative block and bilevel

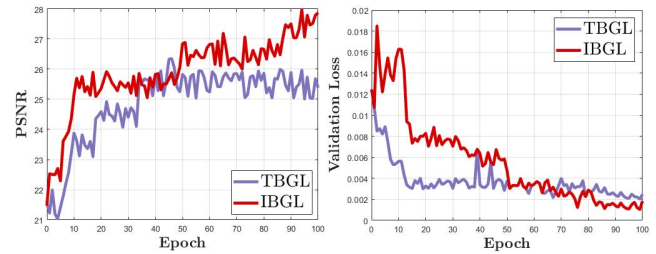


Figure 6: Comparison results of the TBGL and IBGL by analysing the PSNR and validation loss during the training.

Table 3: Verifying the generalization of GB trained on different basic tasks. “GB”, “EN”, “DE”, “SE” represent the generative block, enhancement task, detection task and segmentation task, respectively.

Model	Basic Task		Learning Strategy		EN		DE		SE	
	EN	DE	Naive	IBGL	NIQE \downarrow	LOE \downarrow	mAP \uparrow	mIOU \uparrow	mAP \uparrow	mIOU \uparrow
M_a	\times	\checkmark	\checkmark	\times	4.52	103.72	0.664	42.31		
M_b	\times	\checkmark	\times	\checkmark	4.35	94.75	0.671	43.31		
M_c	\checkmark	\times	\checkmark	\times	4.30	114.62	0.683	44.15		
M_d	\checkmark	\times	\times	\checkmark	3.93	76.96	0.690	44.91		

learning. When GB are trained on various tasks, we embed them directly into other tasks while keeping their parameters frozen. It is clear that the GB trained on the enhancement task achieves excellent results on other vision tasks. As shown in Fig. 8 and Fig. 9, our method outperforms M_b in terms of face detection task, as it can detect a greater number of faces. Additionally, our scheme exhibits higher accuracy in the segmentation task compared to M_c . According to the Table. 3, our method delivers a significant improvement in mAP and mIOU, boosting them by 3.6% and 4.5% respectively in comparison to M_b . Our method demonstrates superior performance to the naive approach, with the 4.3% mAP and 2.1% mIOU increase

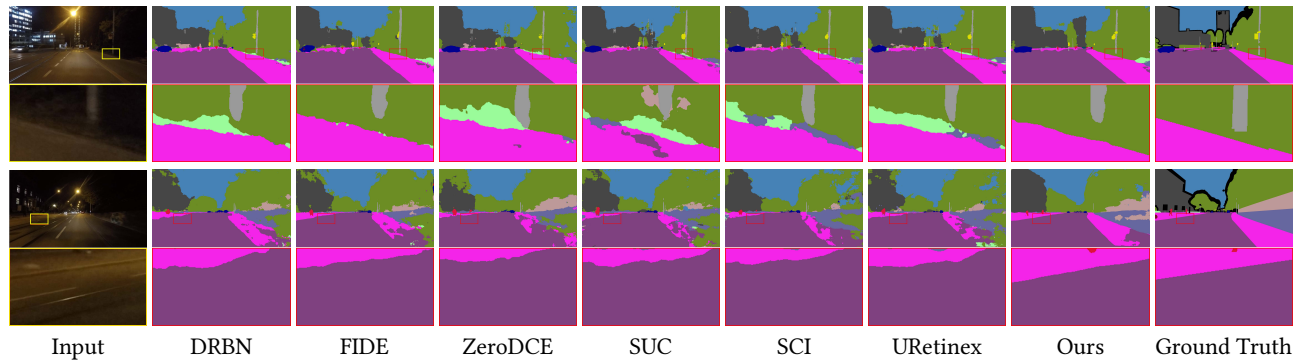


Figure 7: Visual comparison results against state-of-the-art low-light image enhancement approaches on the ACDC dataset.

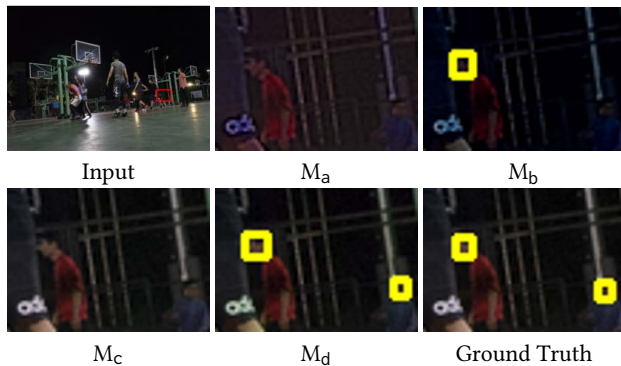


Figure 8: Comparative analysis of dark face detection results using various training strategies and vision tasks on the DARK FACE dataset .

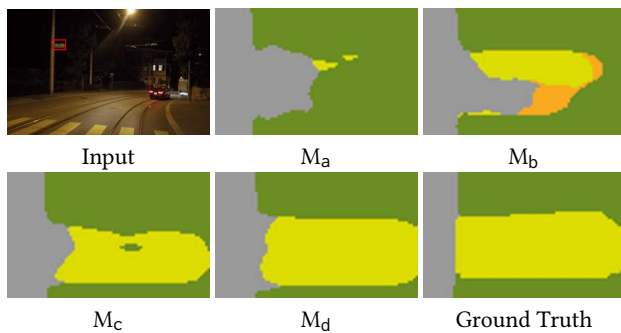


Figure 9: Comparative analysis of low-light semantic segmentation results using various training strategies and vision tasks on the ACDC dataset.

for both the detection and segmentation tasks. Through our analysis, we have discovered that training on enhancement task can facilitate the learning of scene information that is transferable to a range of vision tasks. Our bilevel training strategy is particularly effective in highlighting this generalization.

Analysis of the training strategies. In this section, we evaluated our proposed demand-oriented learning strategy with two variants,

TBGL and IBGL. Fig. 5 demonstrates that IBGL outperforms the TBGL methods in restoring texture details. For example, the text of IBGL is clearer, while the effect of TBGL is more blurred in the zoomed-in area in the first row. From the numerical results as shown in Table. 4, IBGL achieved an improvement of almost 0.639 dB in PSNR than TBGL. The last row in the table shows that IBGL demands more accurate computations and utilizes a greater amount of memory space. Fig. 6 depicts the different training trends for PSNR and validation loss after approximately 500 epochs during the warm start phase. IBGL is more convergent than TBGL, it demonstrated better accuracy.

Table 4: Comparison of quantitative results of IBGL and TBGL on the SID dataset. Three metrics (*i.e.*, PSNR, SSIM, LPIPS) are reported, Mb for GPU Usage.

Strategy	PSNR \uparrow	SSIM \uparrow	LPIPS \downarrow	GPU Usage \downarrow
TBGL	28.483	0.753	0.667	5781
IBGL	29.122	0.769	0.432	12605

5 CONCLUSION

In this paper, we have proposed a unified framework to address diverse low-light vision tasks. By introducing GB from the RAW domain space, we have constructed a common low-light observation that connects different vision tasks. The inner relationship of them is seldom considered. Through imposing learnable data generation, we have formulated a bilevel generative modeling approach. Additionally, we have proposed two practical strategies to effectively address real-world demands. The comprehensive ability of our framework has been demonstrated through two representative low-light vision tasks, namely detection and segmentation, achieving state-of-the-art results.

ACKNOWLEDGEMENTS

This work is partially supported by the National Key R&D Program of China (No. 2022YFA1004101), the National Natural Science Foundation of China (No. U22B2052).

REFERENCES

- [1] Chen Chen, Qifeng Chen, Jia Xu, and Vladlen Koltun. 2018. Learning to see in the dark. In *IEEE CVPR*. 3291–3300.
- [2] Linwei Chen, Ying Fu, Kaixuan Wei, Dezhi Zheng, and Felix Heide. 2023. Instance Segmentation in the Dark. *arXiv preprint arXiv:2304.14298* (2023).
- [3] Liang-Chieh Chen, Yukun Zhu, George Papandreou, Florian Schroff, and Hartwig Adam. 2018. Encoder-decoder with atrous separable convolution for semantic image segmentation. In *ECCV*. 801–818.
- [4] Ziteng Cui, Guo-Jun Qi, Lin Gu, Shaodi You, Zenghui Zhang, and Tatsuya Harada. 2021. Multitask aet with orthogonal tangent regularity for dark object detection. In *IEEE CVPR*. 2553–2562.
- [5] Xingbo Dong, Wanyan Xu, Zhihui Miao, Lan Ma, Chao Zhang, Jiewen Yang, Zhe Jin, Andrew Beng Jin Teoh, and Jiajun Shen. 2022. Abandoning the Bayer-filter to see in the dark. In *IEEE CVPR*. 17431–17440.
- [6] Ian Goodfellow, Jean Pouget-Abadie, Mehdi Mirza, Bing Xu, David Warde-Farley, Sherjil Ozair, Aaron Courville, and Yoshua Bengio. 2020. Generative adversarial networks. *Commun. ACM* 63, 11 (2020), 139–144.
- [7] Shuhang Gu, Yawei Li, Luc Van Gool, and Radu Timofte. 2019. Self-guided network for fast image denoising. In *IEEE CVPR*. 2511–2520.
- [8] Chunle Guo, Chongyi Li, Jichang Guo, Chen Change Loy, Junhui Hou, Sam Kwong, and Runmin Cong. 2020. Zero-reference deep curve estimation for low-light image enhancement. In *IEEE CVPR*. 1780–1789.
- [9] Jie Huang, Yajing Liu, Feng Zhao, Keyu Yan, Jinghao Zhang, Yukun Huang, Man Zhou, and Zhiwei Xiong. 2022. Deep fourier-based exposure correction network with spatial-frequency interaction. In *ECCV*. Springer, 163–180.
- [10] Jie Huang, Man Zhou, Yajing Liu, Mingde Yao, Feng Zhao, and Zhiwei Xiong. 2022. Exposure-consistency representation learning for exposure correction. In *ACM MM*. 6309–6317.
- [11] Henry Alexander Ignatious, Manzoor Khan, et al. 2022. An overview of sensors in Autonomous Vehicles. *Procedia Computer Science* 198 (2022), 736–741.
- [12] Yifan Jiang, Xinyu Gong, Ding Liu, Yu Cheng, Chen Fang, Xiaohui Shen, Jianchao Yang, Pan Zhou, and Zhangyang Wang. 2021. Enlightengan: Deep light enhancement without paired supervision. *IEEE TIP* 30 (2021), 2340–2349.
- [13] Dian Jin, Long Ma, Risheng Liu, and Xin Fan. 2021. Bridging the gap between low-light scenes: Bilevel learning for fast adaptation. In *ACM MM*. 2401–2409.
- [14] Mohit Lamba, Atul Balaji, and Kaushik Mitra. 2020. Towards fast and light-weight restoration of dark images. *arXiv preprint arXiv:2011.14133* (2020).
- [15] Mohit Lamba and Kaushik Mitra. 2021. Restoring extremely dark images in real time. In *IEEE CVPR*. 3487–3497.
- [16] Jiawei Li, Jinyuan Liu, Shihua Zhou, Qiang Zhang, and Nikola K Kasabov. 2022. Learning a coordinated network for detail-refinement multiexposure image fusion. *IEEE TCSVT* 33, 2 (2022), 713–727.
- [17] Jian Li, Yabiao Wang, Changan Wang, Ying Tai, Jianjun Qian, Jian Yang, Chengjie Wang, Jilin Li, and Feiyue Huang. 2019. DSFD: dual shot face detector. In *IEEE CVPR*. 5060–5069.
- [18] Jinxu Liang, Jingwen Wang, Yuhui Quan, Tianyi Chen, Jiaying Liu, Haibin Ling, and Yong Xu. 2021. Recurrent exposure generation for low-light face detection. *IEEE TMM* 24 (2021), 1609–1621.
- [19] Jinyuan Liu, Xin Fan, Ji Jiang, Risheng Liu, and Zhongxuan Luo. 2021. Learning a deep multi-scale feature ensemble and an edge-attention guidance for image fusion. *IEEE TCSVT* 32, 1 (2021), 105–119.
- [20] Jinyuan Liu, Jingjie Shang, Risheng Liu, and Xin Fan. 2022. Attention-guided global-local adversarial learning for detail-preserving multi-exposure image fusion. *IEEE TCSVT* 32, 8 (2022), 5026–5040.
- [21] Jinyuan Liu, Guanyao Wu, Junsheng Luan, Zhiying Jiang, Risheng Liu, and Xin Fan. 2023. HoLoCo: Holistic and local contrastive learning network for multi-exposure image fusion. *Information Fusion* 95 (2023), 237–249.
- [22] Risheng Liu, Jiaxin Gao, Xuan Liu, and Xin Fan. 2022. Revisiting GANs by Best-Response Constraint: Perspective, Methodology, and Application. *arXiv preprint arXiv:2205.10146* (2022).
- [23] Risheng Liu, Zhiying Jiang, Xin Fan, and Zhongxuan Luo. 2019. Knowledge-driven deep unrolling for robust image layer separation. *IEEE TNNLS* 31, 5 (2019), 1653–1666.
- [24] Risheng Liu, Jinyuan Liu, Zhiying Jiang, Xin Fan, and Zhongxuan Luo. 2020. A bilevel integrated model with data-driven layer ensemble for multi-modality image fusion. *IEEE TIP* 30 (2020), 1261–1274.
- [25] Risheng Liu, Zhu Liu, Jinyuan Liu, Xin Fan, and Zhongxuan Luo. 2023. A Task-guided, Implicitly-searched and Meta-initialized Deep Model for Image Fusion. *arXiv preprint arXiv:2305.15862* (2023).
- [26] Risheng Liu, Long Ma, Tengyu Ma, Xin Fan, and Zhongxuan Luo. 2022. Learning with nested scene modeling and cooperative architecture search for low-light vision. *IEEE TPAMI* (2022).
- [27] Risheng Liu, Long Ma, Jiaao Zhang, Xin Fan, and Zhongxuan Luo. 2021. Retinex-inspired unrolling with cooperative prior architecture search for low-light image enhancement. In *IEEE CVPR*. 10561–10570.
- [28] Zhu Liu, Jinyuan Liu, Guanyao Wu, Xin Fan, and Risheng Liu. 2023. Embracing Compact and Robust Architectures for Multi-Exposure Image Fusion. *arXiv preprint arXiv:2305.12236* (2023).
- [29] Zhu Liu, Jinyuan Liu, Guanyao Wu, Long Ma, Xin Fan, and Risheng Liu. 2023. Bi-level Dynamic Learning for Jointly Multi-modality Image Fusion and Beyond. *IJCAI* (2023).
- [30] Long Ma, Dian Jin, Nan An, Jinyuan Liu, Xin Fan, and Risheng Liu. 2023. Bilevel Fast Scene Adaptation for Low-Light Image Enhancement. *arXiv preprint arXiv:2306.01343* (2023).
- [31] Long Ma, Tengyu Ma, Risheng Liu, Xin Fan, and Zhongxuan Luo. 2022. Toward fast, flexible, and robust low-light image enhancement. In *IEEE CVPR*. 5637–5646.
- [32] Steven Macenski, Tully Foote, Brian Gerkey, Chris Lalancette, and William Woodall. 2022. Robot Operating System 2: Design, architecture, and uses in the wild. *Science Robotics* 7, 66 (2022), eabm6074.
- [33] Paras Maharjan, Li Li, Zhu Li, Ning Xu, Chongyang Ma, and Yue Li. 2019. Improving extreme low-light image denoising via residual learning. In *IEEE ICME*. IEEE, 916–921.
- [34] Anish Mittal, Anush Krishna Moorthy, and Alan Conrad Bovik. 2012. No-reference image quality assessment in the spatial domain. *IEEE TIP* 21, 12 (2012), 4695–4708.
- [35] Anish Mittal, Rajiv Soundararajan, and Alan C Bovik. 2012. Making a “completely blind” image quality analyzer. *IEEE SPL* 20, 3 (2012), 209–212.
- [36] Christos Sakaridis, Dengxin Dai, and Luc Van Gool. 2021. ACDC: The adverse conditions dataset with correspondences for semantic driving scene understanding. In *IEEE ICCV*. 10765–10775.
- [37] Hamid R Sheikh and Alan C Bovik. 2006. Image information and visual quality. *IEEE TIP* 15, 2 (2006), 430–444.
- [38] Di Wang, Jinyuan Liu, Risheng Liu, and Xin Fan. 2023. An interactively reinforced paradigm for joint infrared-visible image fusion and saliency object detection. *Information Fusion* 98 (2023), 101828.
- [39] Shuhang Wang, Jin Zheng, Hai-Miao Hu, and Bo Li. 2013. Naturalness preserved enhancement algorithm for non-uniform illumination images. *IEEE TIP* 22, 9 (2013), 3538–3548.
- [40] Wenjing Wang, Xinhao Wang, Wenhan Yang, and Jiaying Liu. 2022. Unsupervised Face Detection in the Dark. *IEEE TPAMI* (2022).
- [41] Chen Wei, Wenjing Wang, Wenhan Yang, and Jiaying Liu. 2018. Deep retinex decomposition for low-light enhancement. *arXiv preprint arXiv:1808.04560* (2018).
- [42] Wenhui Wu, Jian Wang, Pingping Zhang, Xu Wang, Wenhan Yang, and Jianmin Jiang. 2022. Uretinex-net: Retinex-based deep unfolding network for low-light image enhancement. In *IEEE CVPR*. 5901–5910.
- [43] Ke Xu, Xin Yang, Baocai Yin, and Rynson WH Lau. 2020. Learning to restore low-light images via decomposition-and-enhancement. In *IEEE CVPR*. 2281–2290.
- [44] Wanyan Xu, Xingbo Dong, Lan Ma, Andrew Beng Jin Teoh, and Zhixian Lin. 2022. RawFormer: An Efficient Vision Transformer for Low-Light RAW Image Enhancement. *IEEE SPL* 29 (2022), 2677–2681.
- [45] Xiaogang Xu, Ruixing Wang, Chi-Wing Fu, and Jiaya Jia. 2022. SNR-aware low-light image enhancement. In *IEEE CVPR*. 17714–17724.
- [46] Wenhan Yang, Shiqi Wang, Yuming Fang, Yue Wang, and Jiaying Liu. 2020. From fidelity to perceptual quality: A semi-supervised approach for low-light image enhancement. In *IEEE CVPR*. 3063–3072.
- [47] Wenhan Yang, Ye Yuan, Wenqi Ren, Jiaying Liu, Walter J Scheirer, Zhangyang Wang, Taiheng Zhang, Qiaoyong Zhong, Di Xie, Shiliang Pu, et al. 2020. Advancing image understanding in poor visibility environments: A collective benchmark study. *IEEE TIP* 29 (2020), 5737–5752.
- [48] Jinghao Zhang, Jie Huang, Mingde Yao, Man Zhou, and Feng Zhao. 2022. Structure- and Texture-Aware Learning for Low-Light Image Enhancement. In *ACM MM*. 6483–6492.
- [49] Lin Zhang, Lei Zhang, Xuanqin Mou, and David Zhang. 2011. FSIM: A feature similarity index for image quality assessment. *IEEE TIP* 20, 8 (2011), 2378–2386.
- [50] Richard Zhang, Phillip Isola, Alexei A Efros, Eli Shechtman, and Oliver Wang. 2018. The unreasonable effectiveness of deep features as a perceptual metric. In *IEEE CVPR*. 586–595.
- [51] Yonghua Zhang, Xiaojie Guo, Jiayi Ma, Wei Liu, and Jiawan Zhang. 2021. Beyond brightening low-light images. *IJCV* 129 (2021), 1013–1037.
- [52] Yihua Zhang, Guanhua Zhang, Prashant Khanduri, Mingyi Hong, Shiyu Chang, and Sijia Liu. 2022. Revisiting and advancing fast adversarial training through the lens of bi-level optimization. In *ICML*. PMLR, 26693–26712.
- [53] Yonghua Zhang, Jiawan Zhang, and Xiaojie Guo. 2019. Kindling the darkness: A practical low-light image enhancer. In *ACM MM*. 1632–1640.